

CLAWAR 2017: 20th International Conference on Climbing and Walking Robots and the Support Technologies for Mobile Machines, Porto, Portugal, 11-13 September 2017.

1

3D-PRINTED LOW-COST MODULAR FORCE SENSORS

F. WASSERFALL, N. HENDRICH, F. FIEDLER and J. ZHANG

*Department of Informatics, University of Hamburg, Germany.**

E-mail: {wasserfall,hendrich,ofiedler,zhang}@informatik.uni-hamburg.de

**Supported by the German Research Foundation in project SFB TRR 169.*

Force and tactile sensing is required for robots interacting autonomously with their environment. Unfortunately, most force sensors available today are still too expensive to be deployed on a large scale. In this paper we introduce a modular approach to design and integrate low-cost force and tactile sensors directly into 3D-printed robot parts. Based on commodity optical proximity sensors embedded into deformable cantilever structures, sensitivity and load capacity can be selected in a wide range. Our modular CAD-library allows the designer to interactively dimension and shape the sensor for a given purpose.

Keywords: Force and Tactile Sensing, Bipedal Walking, Rapid Prototyping

1. Introduction

As noted by Cutkowski et.al.,¹ force and tactile sensing has been an active research area for robotics almost as long as computer vision, but it “always seems to be a few years away from widespread utility”. Of course, there is no doubt that force sensing is essential for any system interacting autonomously with its environment, and the role of force and tactile sensing for human walking and fine motor skills is obvious. The problem then is the availability of suitable sensor technologies, robustness, integration, and last but not least, costs.

Strain-gauge force/torque sensors are readily available and provide precise data with low noise and drift. Unfortunately, the cost of these sensors remains high, and the required precision amplifiers make integration into small and mobile robots difficult.² A variety of other sensor types have been studied to measure normal forces applied to a robot part or surface, including force- and piezo-resistive materials³ (e.g. conductive rubber^{4,5} and polymers⁶), magnetic⁷ and capacitive sensors,⁸ and different optical effects due to sensor deformation.^{9,10}

The wide availability of 3D-printing allows researchers and engineers to integrate force sensing elements seamlessly into a variety of parts and objects.

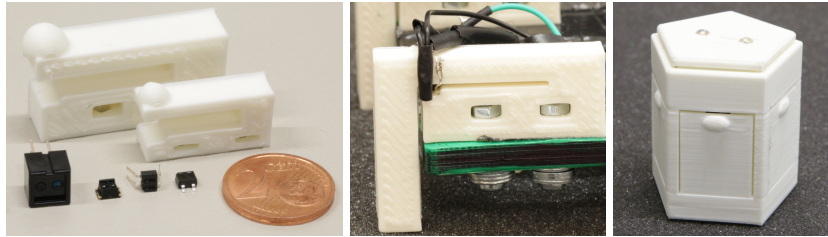


Fig. 1. Different types of optical proximity sensors and two printed push-type cantilevers (left). Pull-type sensor where the beam separates from the proximity sensor with applied force (middle). Instrumented object to measure and record forces induced by human in-hand manipulation operations (right).

Kesner et al.¹¹ summarize the key design principles of a flexure element, a strain transducer to measure deformations and a protective hull. The key advantages of printable force sensors are the ease of integration into small or complex geometries, and a very low price. As summarized in Table 1, using a force-sensing foot for a humanoid robot as an example, total sensor system costs are significantly lower than comparable approaches.

2. Concept

The (well known) basic principle of the proposed sensor is a deformable cantilever. If the mechanical properties of the structure are known, the force inducing the deformation can be computed. Low-cost optical proximity sensors are used to measure the deflection. The sensors (e.g. Everlight ITR8307) consist of an IR-LED transmitter and a photo-transistor, changing its resistivity depending on the reflection of emitted IR-light. Also, the sensors can be directly connected to the built-in analog-digital converters of microcontrollers without external amplifiers. Figure 2 shows the sensor response to changes in the distance to a printed, flat plastic surface.

Table 1. Example configurations and costs for two humanoid robot feet

Configuration	Parts	Qty	Est. cost	Sum
Professional	ATI Nano-17 6-DOF	2	~5000\$	10000\$
FSR sensor set	Robotis OP2-FSR set	1	~450\$	450\$
Load cells	Load cell TAL220	8	~7\$	132\$
	Amplifier HX711	8	~7\$	
	Arduino Pro Mini	2	~10\$	
FSR sensors	Interlink FSR 400	8	~7\$	76\$
	Arduino Pro Mini	2	~10\$	
Printed sensor	ITR8307 optical prox. sensor	8	~0.5\$	24\$
	Arduino Pro Mini	2	~10\$	

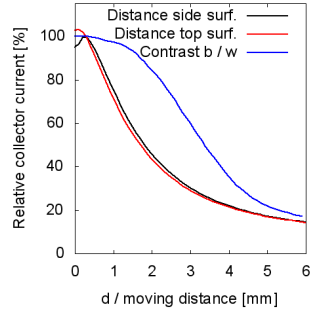


Fig. 2. Characteristics of the Everlight ITR8307 proximity sensor measured against printed plastic surfaces. The distance measurements were taken against the side (black) and top (red) of a white 3D-printed object to evaluate the effect of differently textured surfaces.

with load $q(x)$ is described by the Euler-Bernoulli beam equation,

$$\frac{d^2}{dx^2} \left(EI \frac{d^2 \omega}{dx^2} \right) = q(x) \quad (1)$$

where E describes Young's modulus and I is the beams second moment of area. For the special case of a simply supported beam with point load F applied at a distance l , the deflection $s = \omega(l)$ of the beam at the sensors contact point can be calculated as

$$s = \frac{l^3 F}{3EI} \quad (2)$$

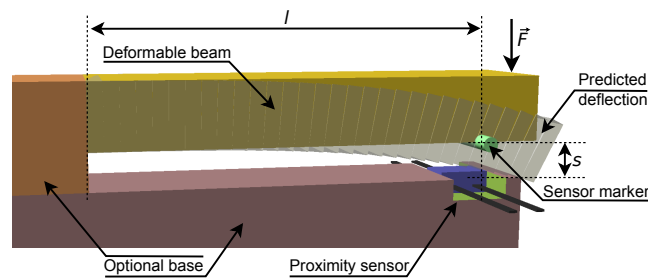


Fig. 3. OpenSCAD rendering of the basic one dimensional push-force sensor, with the deformable beam on top and above the optical proximity sensor. To help the designer to dimension and align the sensor, the rendering optionally also includes the sensor marker (green), the fully deflected beam (gray), and a model of the proximity sensor (blue).

Using these equations, we created parameterizable OpenSCAD modules which can be combined to dynamically compile a sensor for a specific purpose. This can also be used to integrate the sensor directly into a design as demonstrated below. To generate a one-dimensional sensor, the user needs to provide the maximum expected force, beam length and (optionally) beam width. From the area moment of inertia of a rectangular beam $I_x = bh^3/12$ and equation 2 follows the required height of the beam as:

$$h = \sqrt[3]{4 \frac{l^3 F}{Esb}} \quad (3)$$

The maximum deflection s depends on the type of the sensor (push, pull or both) and is a combination of the proximity sensors' minimal distance and sensing range. The basic beam is then used to assemble more sophisticated designs, such as the sensors used for humanoid robot walking described in section 6 or the sensing object for human grasp analysis in section 7.

3. 3D-Printing functional parts

All mechanical sensor parts were printed on different types of FDM printers with commercial PLA- or ABS-filament. As stated in section 2, deformation of the flexible sensor part depends on the geometry and the material's elasticity, described by Young's modulus E , which depends on the printing material. To determine the material's E moduli, we printed a set of test specimen, each consisting of three beams with varying cross sections. E was measured using a modified milling machine and digital scales. The scales' deflection offset was calibrated initially to allow for precise measurements of deflection to force. Young's modulus was then determined by rearranging equation 2 and measuring force F and deflection s .

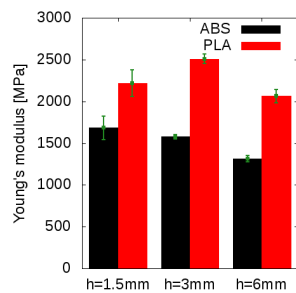


Fig. 4. Young's modulus measured from the 1.5, 3.0 and 6.0m high beams of ABS and PLA.

The results are shown in Fig. 4. The Young's modulus is found to be in the expected range, but is subject to surprisingly high variation. The Young's modulus of FDM-printed ABS parts is reported to be in the range of 1300 to 1900 MPa¹² and 1800 MPa respectively¹³ in the literature. However, the variance of the reported values is induced by the use of different printers; it is not stated how printing different geometries with a single machine would affect the variance.

4. Sensor Calibration

Since the 3D-printed sensors are usually designed for a special purpose and geometry, an easy calibration procedure is crucial. The calibration should be feasible without expensive tools, so as to make the sensors accessible to most researchers and even hobbyists. Direct mapping of applied forces to measured A/D-values from the microcontroller can be done quickly with digital scales or another force sensor and any kind of linear guiding, notably with a 3D-Printer which basically consists of linear guidings. The recorded values are then uploaded as an interpolation table to the microcontroller. However, results obtained in this way are specific to each sensor due to the nonlinear response of the proximity sensors (Fig. 2).

To resolve this issue, the proximity sensor's response can be recorded for a specific surface (color and texture) by moving it along the surface normal (with a 3D-Printer). Indirect mapping now uses this distance table to translate the A/D-values to a deflection for every sensor printed from this particular material. Considering the plastic material's deformation to be linear-elastic according to Hooke's law for small strains, the deflection is directly proportional to the applied force with the spring constant k . Only k and a zero-point calibration is then required to compute the actual force values for a particular sensor.

5. Sensor Accuracy and Resolution

Actual sensor output depends on the used A/D converter and the effective voltage swing generated by the proximity sensor, which in turn depends on the the sensor type (push or pull geometry), maximum cantilever deflection, infrared LED supply current, and effective shielding of ambient light.

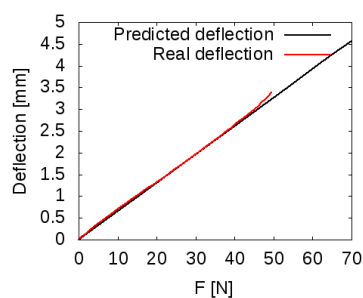


Fig. 5. Comparison of predicted and real deflection for a one-dimensional sensor.

The *resolution* is nonlinear over the sensor's effective range due to the characteristics of the proximity sensor (Fig. 2). For example, a prototype 50 N sensor connected to a 12 bit ADC achieved a resolution between 0.0134 N/bit to 0.075 N/bit over its sensitivity range. These values are computed by the ratio of force to bits from the sensor's calibration table at the upper and lower end of the resolution.

The signal's standard deviation was measured to be in the range of 1-2 bit. By applying a median- or floating-average-filter, the *accuracy* is maintained better than ± 1.5 bit. Maintaining the $\text{SNR} < 1$, this equates to an average resolution of $\frac{0.0134+0.075}{2} \times 1.5 \approx 0.066$ N for a conservative estimation of the standard deviation.

The accuracy of the computational model was evaluated by comparing the predicted deflection for a generated sensor geometry to the measured real deflection after printing the object. The measurement was conducted by mounting the sensor to a 3D-Printer and moving it against a calibrated digital scales as described in section 3. As the result in Fig. 5 shows, the prediction is surprisingly accurate.

6. Humanoid Foot Sensor

We integrated a set of 3D-printed force sensors into our custom RoboCup soccer robot "Hambot",¹⁴ with one sensor in each corner of the likewise 3D-printed feet (Fig. 6). The sensors were designed to reach their full-range deflection at 50 N, so as to support the peak forces which will arise while walking. By combining the readings of each sensor it is possible to calculate the total force on the foot and then the center of pressure (COP).¹⁵ With the COP known, one can determine if the robot stands stable, and correct deviations by keeping the COP close to the center of the foot.

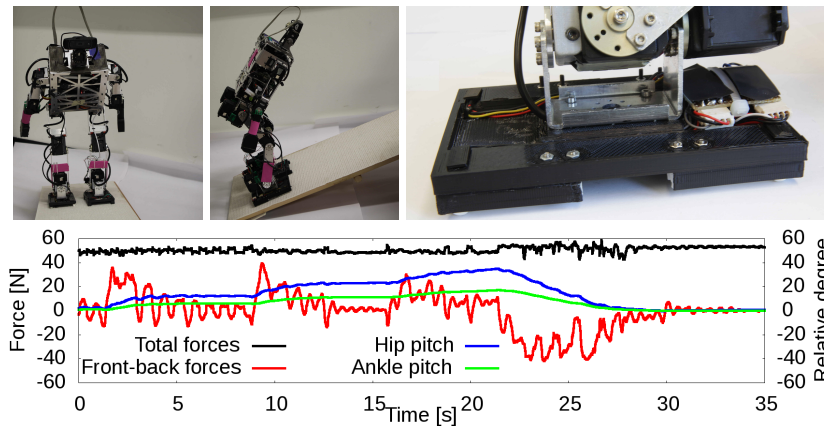


Fig. 6. The Hambot robot while adapting to a tilted ground (left and center), 3D-printed foot of the robot with four force sensors enclosed by light shielding hulls at each corner (right). Force sensor data and the rotation of the pitch motors while the robot is balancing and adapting to the tilted ground (bottom).

To evaluate the performance of the sensors and the general suitability for walking and stabilization tasks, we created a test scenario with the robot balancing on a tilted ground. The robot is stabilizing itself using a PID-controller based approach, which controls the position of the hip-pitch and ankle-pitch. Figure 6 shows the robot adapting to a moving surface. The position of the hip and ankle pitch is plotted against the difference between the sensors in the front and back of the robot and the sum of all eight sensors. The peaks at second 2, 9 and 16 indicate a fast tilting movement of the ground, the smoother gradient from second 22 to 27 is caused by a slow continuous movement. It is notable that the absolute sum of forces on all eight sensors is very accurate although the distribution of the forces differs vastly in time. The variation of the relative front-back forces was caused by flexibility of the robot, resulting in an oscillating force distribution. The controller was also implemented for the robot roll (left-right) dimension with similar performances.

7. Instrumented Objects for Grasp Analysis

Performing dexterous in-hand manipulation tasks with multi-fingered hands is an active research topic. One promising approach is to learn basic movement patterns by generalizing from human demonstrations. This requires a precise tracking of the human hands and the resulting object movements. As finger forces cannot be measured easily on the human hands, the use of force- and motion-sensing objects is an attractive alternative.¹⁶

To record object rotation tasks with finger gaiting, we are currently designing and testing several such objects with different shapes and sizes (Fig. 1 and 7). The surface of the printed object consists of several force sensors. While the geometry of the sensor surfaces is determined by the object-shape, the desired sensor sensitivity is achieved by the adaptive beam computation. Figure 7 shows a pentagon-shaped instrumented object in use.

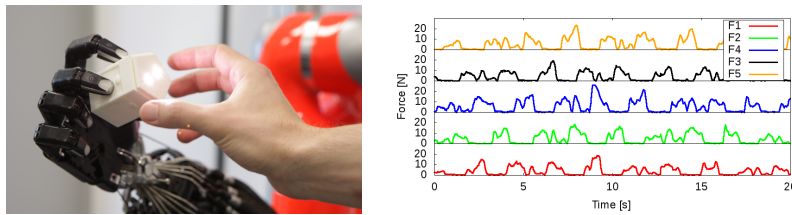


Fig. 7. (left) application of instrumented object to track human-robot handover tasks; (right) forces recorded while rotating the object in one human hand.

8. Conclusion

In this paper, we suggest a family of low-cost force sensors for direct integration into 3D-printed robot parts, supported by a CAD tool that calculates and generates the required cantilever structures. The sensors use commodity optical proximity sensors, are reliable, interface to common microcontrollers without the need for additional electronics or complex amplifiers, and are easy to produce and calibrate with standard 3D-printers: making affordable force sensing available to most researchers. We presented several design examples, and our sensors proved to be durable and reliable when tested on humanoid robots under stressful circumstances (Robocup).

References

1. M. R. Cutkosky, R. D. Howe and W. R. Provancher, Force and tactile sensors, *Springer Handbook of Robotics*, 455 (2008).
2. D. Perry, Multi-axis force and torque sensing, *Sensor Review* **17**, 117 (1997).
3. J. T. Muth *et al.*, Embedded 3D printing of strain sensors within highly stretchable elastomers, *Advanced Materials*, 6307 (2014).
4. M. Shimojo, T. Araki, A. Ming and M. Ishikawa, A ZMP sensor for a biped robot, *IEEE ICRA* (2006).
5. Y. Takahashi, K. Nishiwaki, S. Kagami, H. Mizoguchi and H. Inoue, High-speed pressure sensor grid for humanoid robot foot, in *IEEE IROS*, 2005.
6. S. J. Leigh *et al.*, A Simple, Low-Cost Conductive Composite Material for 3D Printing of Electronic Sensors, *PLoS ONE* **7**(11 2012).
7. S. C. Gomez, M. Vona and D. Kanoulas, A three-toe biped foot with Hall-effect sensing, *IEEE IROS*, 360 (2015).
8. R. Bekhti, V. Duchaine and P. Cardou, Miniature Capacitive Three-Axis Force Sensor, in *IEEE IROS*, 2014.
9. Y. L. Park *et al.*, Force sensing robot fingers using embedded fiber Bragg grating sensors and shape deposition manufacturing, *IEEE ICRA* (2007).
10. K. Willis *et al.*, Printed optics: 3D printing of embedded optical elements for interactive devices, *Proceedings of the 25th annual ACM UIST*, 589 (2012).
11. S. Kesner and R. Howe, Design Principles for Rapid Prototyping Force Sensors using 3D Printing., *IEEE/ASME transactions on mechatronics* (2011).
12. E. Ebel and T. Sinnemann, Fabrication of FDM 3D objects with ABS and PLA and determination of their mechanical properties, *RTejournal* (2014).
13. B. Tymrak, M. Kreiger and J. Pearce, Mechanical properties of components fabricated with open-source 3D printers [...], *Materials & Design* **58** (2014).
14. M. Bestmann, B. Reichardt and F. Wasserfall, Hambot: An open source robot for robocup soccer., in *19th RoboCup international Symposium, Hefei*, 2015.
15. M. Shimojo, T. Araki, A. Ming and M. Ishikawa, A ZMP sensor for a biped robot, in *IEEE ICRA*, May 2006.
16. W. Memberg and P. Crago, Instrumented objects for quantitative evaluation of hand grasp, *Journal of Rehabilitation Research and Development* (1997).